Localization of random walks to competing manifolds of distinct dimensions

Raz Halifa Levi,[1,*] Yacov Kantor,[1] and Mehran Kardar[2]
[1]*Raymond and Beverly Sackler School of Physics and Astronomy, Tel Aviv University, Tel Aviv 69978, Israel*
[2]*Massachusetts Institute of Technology, Department of Physics, Cambridge, Massachusetts 02139, USA*

(Received 7 June 2018; revised manuscript received 23 July 2018; published 8 August 2018)

We consider localization of a random walk (RW) when attracted or repelled by multiple extended manifolds of different dimensionalities. In particular, we consider a RW near a rectangular wedge in two dimensions, where the (zero-dimensional) corner and the (one-dimensional) wall have competing localization properties. This model applies also (as cross section) to an ideal polymer attracted to the surface or edge of a rectangular wedge in three dimensions. More generally, we consider $(d-1)$- and $(d-2)$-dimensional manifolds in d-dimensional space, where attractive interactions are (fully or marginally) relevant. The RW can then be in one of four phases where it is localized to neither, one, or both manifolds. The four phases merge at a special multicritical point where (away from the manifolds) the RW spreads diffusively. Extensive numerical analyses on two-dimensional RWs confined inside or outside a rectangular wedge confirm general features expected from a continuum theory, but also exhibit unexpected attributes, such as a reentrant localization to the corner while repelled by it.

DOI: 10.1103/PhysRevE.98.022108

I. INTRODUCTION

Random walks (RWs) are ubiquitous in physics, modeling myriad systems from diffusion to polymers [1–3]. They are the prototype of scale invariant phenomena, spanning up to a typical size (e.g., root mean square end to end distance) R that scales with the number of steps N as $R \sim N^{\nu_{\rm RW}}$ with $\nu_{\rm RW} = \frac{1}{2}$ in *free space*. This scale invariance is potentially broken in the presence of inhomogeneities (boundaries, obstacles, etc.) that enhance or diminish the weight of RWs passing through different locations. Such weighted RWs may then linger in the vicinity of favorable locales, leading to phenomena such as polymer adsorption to attractive surfaces [4–12], with close analogy to localization of wave functions in quantum bound states [13].

The behavior of polymers near repulsive and attractive *flat* surfaces is well documented. In particular, the value of the critical exponent ν, governing the divergence of the adsorbed layer thickness ξ as the critical adsorption condition is approached, as well as the value of the exponent γ describing the behavior of the partition function at the transition point, are well known for a variety of polymer and solvent types [14]. It has been noted that for nonflat but nevertheless *scale-free* surfaces, such as infinite cones, pyramids, or wedges, the critical exponent γ depends on geometric parameters such as the apex angle of a cone, for both repulsive surfaces [15,16] and attractive surfaces at the transition point [17]. The values of the exponents determine the strength of the forces between the surfaces mediated by flexible polymers. It has also been noted [18] that localized configurations of RWs can be created near an attractive edge between the repulsive walls of a wedge, with an exponent ν governing the divergence of ξ that depends on the opening angle of the wedge.

Our theoretical studies of RWs near scale-free surfaces were originally motivated by the probe shapes used in actual experiments (see, e.g., Ref. [19]). Presence of additional features on the two-dimensional surfaces of the probe, such as one-dimensional edges and zero-dimensional tips, were ignored in these earlier works. Here, we show that these features can result in interesting consequences of their own. In particular, we examine the localization of a RW (idealized polymer) to the surface or edge of a wedge. This serves as the prototype of the more general phase diagram, and multicritical point, that emerges when a RW encounters (weakly) attractive regions of different dimensions.

The paper is organized as follows: The (well-known) localization to the flat boundary of an excluded half-space is reviewed in Sec. II for a lattice realization of weighted RWs. We particularly make note that at the critical weight for delocalization, the RW spreads as in free space, a condition that can be realized for a specific choice of weights with arbitrary boundaries, and that is reminiscent of reflecting boundary conditions in the continuum limit. As discussed in Sec. III, when the boundary is folded into a rectangular wedge (excluded quarter space), we find that the RW may become localized to the corner, while repelled by the rest of the boundary. This suggests a phase diagram with four phases corresponding to bound or unbound states to corner or edge, which is explored in Sec. IV. By considering the continuum limit, we argue that the four phases come together at a novel multicritical point where the polymer behaves as in free space. We conclude with a discussion of possible theoretical extensions and experimental realizations in Sec. V.

In order not to distract from the central narrative, various numerical and analytical details, as well as some pertinent references, are relegated to a number of Appendices. In particular, Appendix A discusses lattice treatment of weighted walks, while Appendix B recounts well-known connections between RWs, quantum mechanics, and polymers in continuous space.

*razhalifa@gmail.com

The latter is important as polymer adsorption provides a possible physical realization of the mathematical results. The discrete implementation of RWs on a square lattice, detailed in Appendix A, is applied to the problem of an attractive layer in Appendix C, and to an attractive rectangular wedge in Appendix D. The distinct numerical signatures of unbounded and localized (to edge or corner) states, as discussed in these Appendices, allow for computation of phase diagrams as described in Appendix E. Localization to the corner in the limit of strong attraction to the boundary can be studied asymptotically as a one-dimensional problem as detailed in Appendices F and G.

II. LOCALIZATION TO A SURFACE

Let us consider RWs on a d-dimensional hypercubic lattice, with lattice constant ℓ. The number of walks of N steps (without any obstacles) grows as $\mathcal{Z}_0 = \mu^N$, where μ is the coordination number (number of nearest neighbors of a site) of a regular lattice. On a hypercubic lattice $\mu = 2d$. This can be generalized to walks on an inhomogeneous lattice with non-negative weights $q(\mathbf{r})$ assigned to every site, leading to a particular N-step walk from $\mathbf{r}_0$ to $\mathbf{r} \equiv \mathbf{r}_N$ acquiring a weight $q(\mathbf{r}_0)q(\mathbf{r}_1)\dots q(\mathbf{r}_N)$. The total weight of all walks from $\mathbf{r}_0$ and to $\mathbf{r}$ will be denoted by $\mathcal{Z}(\mathbf{r}, \mathbf{r}_0, N)$. It is convenient to use the *reduced* weight $\tilde{\mathcal{Z}}(\mathbf{r}, \mathbf{r}_0, N) \equiv \mathcal{Z}(\mathbf{r}, \mathbf{r}_0, N)/\mathcal{Z}_0$, which can be computed recursively as

$$\tilde{\mathcal{Z}}(\mathbf{r}, \mathbf{r}_0, N+1) = \frac{q(\mathbf{r})}{2d} \sum_{\mathbf{r}' \text{ nn of } \mathbf{r}} \tilde{\mathcal{Z}}(\mathbf{r}', \mathbf{r}_0, N), \tag{1}$$

with the starting condition $\tilde{\mathcal{Z}}(\mathbf{r}, \mathbf{r}_0, 0) = q(\mathbf{r}_0)\delta_{\mathbf{r},\mathbf{r}_0}$.

We note the following two interpretations of weighted walks: From the perspective of a diffusing particle, the coordinates $\mathbf{r}_0, \mathbf{r}_1, \dots \mathbf{r}$ represent a time sequence of locations visited starting from $\mathbf{r}_0$ in N steps. In such a model $0 < q < 1$ can be interpreted as a partially absorbing site, $q = 0$ a completely absorbing one, while $q > 1$ represents a site where particles can proportionately increase in number. (Effectively, q represents again along a fixed path in a medium with random amplification and attenuation.) The reduced weight $\tilde{\mathcal{Z}}(\mathbf{r}, \mathbf{r}_0, N)$ will then be proportional to the mean number of particles at position $\mathbf{r}$. Alternatively, the entire walk can represent a configuration of an *ideal polymer* anchored at $\mathbf{r}_0$, with $q(\mathbf{r}) = \exp[-\beta V^{\text{th}}(\mathbf{r})]$ interpreted as the Boltzmann weight of a potential $V^{\text{th}}(\mathbf{r})$. In this case, $q > 1$ models an attractive site, $q < 1$ represents a repulsive potential with $q = 0$ corresponding to an excluded point (hard obstacle). Consequently, $\mathcal{Z}$ and $\tilde{\mathcal{Z}}$ should be interpreted as regular and reduced *partition functions*, that are proportional to the probability of finding the end point of a polymer at $\mathbf{r}$. In this paper we will mostly use terminology appropriate to the polymer interpretation. Further aspects of Eq. (1), specifically as matrix multiplication, are discussed in Appendix A.

Figure 1(a) is an example that uses the recurrence relation (1) on a $d = 2$ square lattice [$\mathbf{r} = (x_1, x_2)$] to calculate $\tilde{\mathcal{Z}}(\mathbf{r}_0, \mathbf{r}, N)$, for a walk anchored at (0,0), and with an excluded half-plane, i.e., $q(\mathbf{r}) = 0$ for $x_1 \leqslant -1$. We can divide lattice sites into "even" ("e") and "odd" ("o") sublattices, depending on whether the sum of their coordinates is even or odd. Note that Eq. (1) connects "e" sites to "o" and vice versa. Therefore, depending on even or odd N, either "o" or "e" sites of the lattice will have vanishing $\tilde{\mathcal{Z}}$. For clarity these "e-o" oscillations are "smoothed out" in all figures showing $\tilde{\mathcal{Z}}$. If an attractive layer is introduced at the boundary of the repulsive region with $q(\mathbf{r} = (0, x_2)) = w > 1$, then, for sufficiently large w, the walks become adsorbed on the boundary, as in Fig. 1(d).

In empty space, i.e., for $q(\mathbf{r}) = 1$ everywhere, Eq. (1) is a discretized diffusion equation, which for large N, disregarding "e-o" oscillations, has a *Gaussian* solution

$$\tilde{\mathcal{Z}}(\mathbf{r}, \mathbf{r}_0, N) \sim \exp\left[-\frac{d(\mathbf{r} - \mathbf{r}_0)^2}{2N}\right]. \tag{2}$$

In the presence of repulsive boundaries, such as hard walls with $q = 0$, the solutions tend to decrease towards the walls, while increasing for attractive potentials with $q > 1$. However, an appropriate combination of an attractive layer of strength w and a repulsive surface can create a *neutral* condition. In Appendix A we show that such neutrality is achieved when Eq. (1) admits a *uniform*N-independent solution $\tilde{\mathcal{Z}}_N = \tilde{\mathcal{Z}}_{N+1} = \psi_{\text{uni}}(\mathbf{r}) = 1$ at any point in space, where $q(\mathbf{r}) > 0$. In particular, for a flat layer in $d = 2$ the *critical value* is $w = w_c = \frac{4}{3}$. For a general flat surface of dimension $D = d - 1$, perpendicular to one of main axes of d-dimensional hypercubic lattice,

$$w_c = 2d/(2d-1), \tag{3}$$

is a well-known result from Rubin [20,21], also derived in Appendix A. For $w = w_c$, the wall becomes *"invisible"* to the polymer. In particular, the presence of the wall does not disturb the free space solution of Eq. (2) in the nonexcluded space, as can be seen in the Gaussian probability density distribution obtained in Fig. 1(c).

As discussed in detail in Ref. [18], under certain conditions, such as with a slow variation of V^{th}, a continuum limit of Eq. (1) can be obtained [22]. Rewriting Eq. (B1) from Appendix B, the simplified continuum form is

$$\frac{\partial \tilde{\mathcal{Z}}}{\partial N} = c\nabla^2 \tilde{\mathcal{Z}} - U\tilde{\mathcal{Z}}, \tag{4}$$

with a dimensionless temperature-dependent potential $U(\mathbf{r}) = \beta V^{\text{th}}(\mathbf{r})$ and a lattice-dependent constant c. This equation is reminiscent of the Schrödinger equation, with N as imaginary time. The long "time" limit is now governed by the ground state of the operator on the right-hand side of Eq. (4). In Appendix B we analyze a particular case of $U(\mathbf{r})$ representing a short-range attractive potential near a $(d-1)$-dimensional repulsive wall, and compare the results with the discrete model from Appendix A. Quantitative analysis of general properties, as well as similarities and subtle differences between the N-dependent solutions in continuum and discrete models, can be found in Appendix C.

In the presence of a repulsive wall with an attractive layer on a lattice (or attractive well in the continuum) the transition between delocalized and adsorbed states occurs at a critical $w_c > 1$ (or for a sufficiently shallow, yet *finite* depth of of the well in the continuum). Since both Boltzmann weight w and the dimensionless potential U depend on the temperature T, we can treat changes of these variables as changes in the temperature for fixed potentials. Thus, the critical potential will correspond to some *adsorption transition temperature*

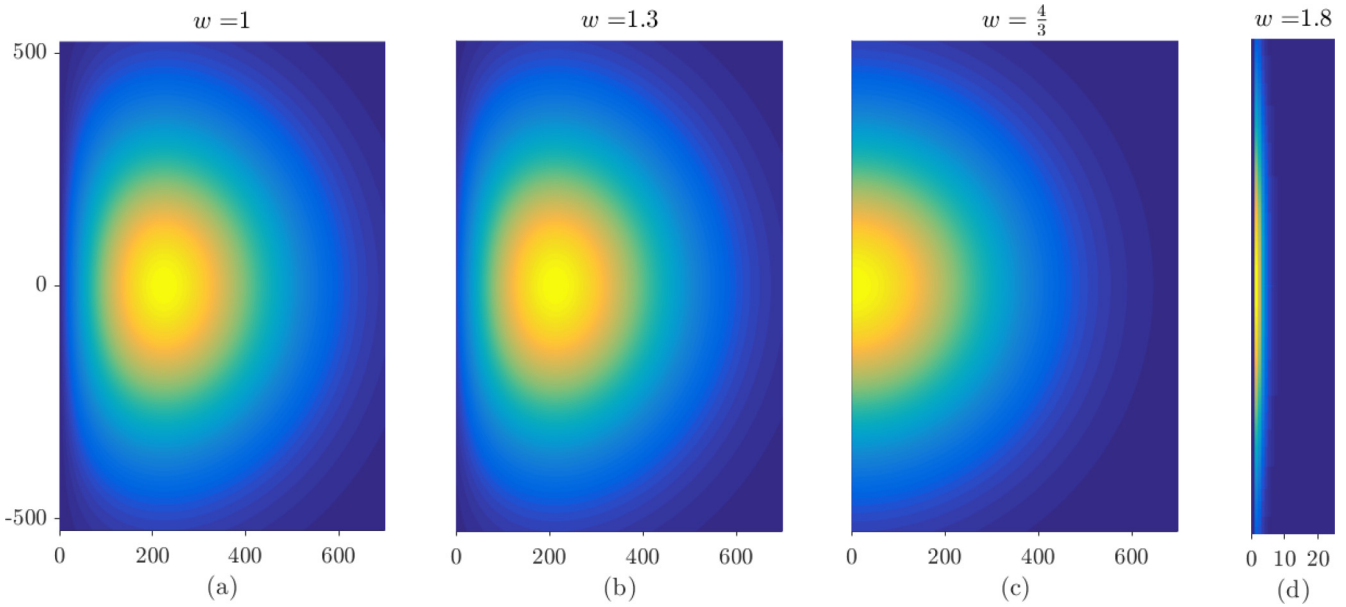

FIG. 1. Reduced partition function $\tilde{\mathcal{Z}}(\mathbf{r}, \mathbf{r}_0, N)$ for a RW that starts at the point $\mathbf{r}_0 = (0, 0)$ as a function of its end position $\mathbf{r}$ for $N = 10^5$ on a square lattice. The excluded half-space is bounded by an attractive layer characterized by Boltzmann weight w, whose value is indicated above each picture. All plots have the same vertical scale centered at the anchoring point. Horizontal scales of (a), (b), and (c) are the same as the vertical scale, while in (d) it is stretched for clarity. Plot (a) corresponds to unweighted exclusion of half the space ($w = 1$). In (b), w is just 0.033 below the localization transition point, but the plot is very similar to (a). Plot (c) shows the Gaussian distribution at the transition point. Plot (d) shows a state for w above the critical point that is adsorbed to the boundary.

T_a, with small deviations from criticality proportional to $\delta T \equiv T_a - T$. Below T_a, the polymer lingers in a layer of characteristic width (localization length) ξ. (While above T_a the polymer is not localized, a corresponding length ξ serves as a crossover scale to the region where the attractive potential is no longer relevant.) Close to the transition temperature, this length diverges as $\xi \sim \delta T^{-\nu}$, with $\nu = 1$ for a planar surface of dimension $D = d - 1$. [See Eq. (B4) in Appendix B, and the numerical confirmation in Appendix C.] The thickness of the adsorbed polymer layer in Fig. 1 decreases rapidly with increased attraction, and is only a few lattice spacings thick for $w = 1.8$. For $w \gtrsim 2$ the RW is practically one dimensional (1D) with most of the weight concentrated in the attracting layer. We note that in the absence of the repulsive wall (no excluded region), the critical depth is zero (i.e., $w_c = 1$), and localization occurs for any attractive potential. Nonetheless, the qualitative behavior near transition remains the same.

The universality of critical behavior near the transition is best analyzed in the continuum limit. Consider a potential that attracts $0 \leqslant C \leqslant d$ coordinates of the walker to the origin. Such an attractive manifold of dimension $D = d - C$ can be modeled in the continuum by a potential $-U(\mathbf{r}) = u_C \delta(x_1)\delta(x_2)\ldots\delta(x_C)$. [In $d = 3$ dimensions, attraction to a surface ($D = 2$), line ($D = 1$), or point ($D = 0$) are described, respectively, with $C = 1$, 2, or 3.] A rescaling of Eq. (4) by $\mathbf{r} \to b\mathbf{r}$ and $N \to b^2 N$ (consistent with $\nu_{\rm RW} = \frac{1}{2}$) leaves the diffusion term invariant but scales the potential to

$$u_C \to b^{2-C} u_C \quad \Rightarrow \quad \frac{d\, u_C}{d \ln b} = (2 - C) u_C. \tag{5}$$

This scaling provides the first term in a renormalization group (RG) flow [23–26]. A weakly attractive potential grows in strength (for $C < 2$) to unity at a scale $\xi \propto u_C^{-\nu}$, with the critical exponent $\nu = 1/(2 - C)$.

Regarding the manifold dimension C as a continuous variable, Eq. (5) shows that u_C grows under scaling for $C < 2$, but decays to zero for $C > 2$. This is a well-known result that even weak attraction or repulsion for $C < 2$ is relevant, leading to bound or scattered states. A numerical illustration of this is presented in Fig. 1 for a lattice implementation of random walks on a square lattice ($d = 2$) with an attractive line ($D = 1$) of points with weight w. Superficially, it may appear that the lattice system depicted in Fig. 1 is quite different from the continuum potential $u_1 \delta(x)$, as the lattice RW is excluded from an entire half-space with $x < 0$. However, this exclusion merely serves to shift the critical value separating scattered and localized states from $w = 1$ ($u_1 = 0$) to $w_c = \frac{4}{3}$. At the critical point, such as depicted in Fig. 1(c), the end point of the RW spreads diffusively (as a half Gaussian), as would be the case for $u_1 = 0$ in the continuum treatment.

III. LOCALIZATION TO A CORNER

Figure 2 depicts what happens when the boundary of Fig. 1 is folded to exclude quarter of the space. The shape of the distribution of the end point of the RW is naturally modified, but a somewhat surprising element is that at the critical value of w_c, the end point does not diffuse as a Gaussian but remains localized to the corner [compare Figs. 1(c) and 2(c)]. A detailed analysis confirming this feature is presented in Appendix D.

The reason for this behavior can be gleaned by examining our implementation of the excluded points and the attractive layer on a discrete lattice. Every point of the attractive layer on a flat surface, depicted in Fig. 3(a), including the blue anchoring

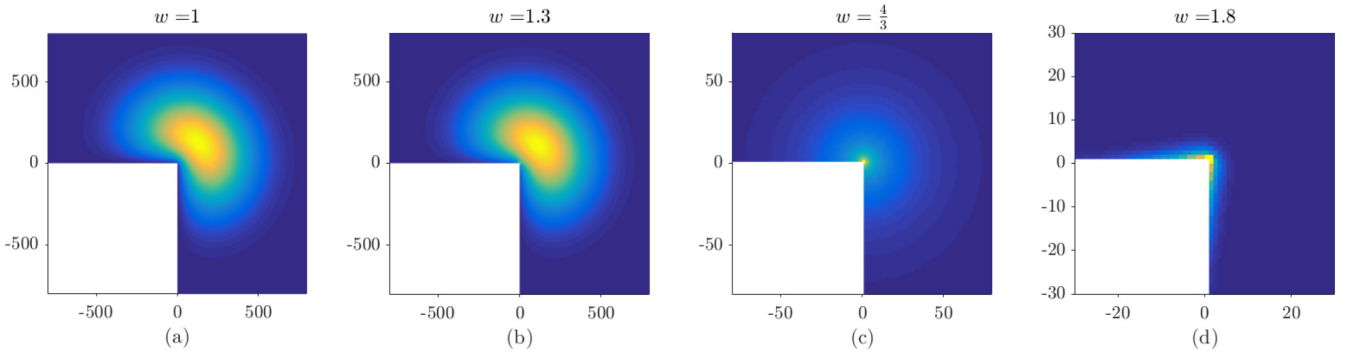

FIG. 2. Reduced partition function $\tilde{\mathcal{Z}}(\mathbf{r}, \mathbf{r}_0, N)$ for a RW that starts at the corner of a repulsive wedge $\mathbf{r}_0 = (0, 0)$ as a function of its end position $\mathbf{r}$ for $N = 10^5$ on a square lattice. The excluded quarter space is bounded by an attractive layer with Boltzmann weight w. (The value of w is indicated above each picture.) The horizontal and vertical scales are equal to each other in every plot. However, each plot has its own scale selected for clearest view of the distribution. Plot (a) corresponds to unweighted exclusion ($w = 1$). While in plot (b) w is 0.033 below the localization transition point in Fig. 1(c), the probability is only slightly distorted form that in (a). At this "transition value" of $w_c = \frac{4}{3}$, the density becomes rotationally symmetric, but clearly remains bounded to the corner. For the stronger value of w in plot (d), the walker while centered at the corner is almost confined to the one-dimensional edge.

point, has three nearest nonexcluded neighbors. However, in case of layers bounding a rectangular wedge, either from outside [Fig. 3(b)] or from inside [Fig. 3(c)], the immediate environment of the corner (anchoring) point is distinct, with four or two neighbors, respectively. In Appendix D we argue that in the situation, the mere excess or deficiency in the number of nearest neighbors generates an effective attractive or repulsive weight for the corners in Figs. 3(b) and 3(c), respectively. In fact, for $w \gtrsim 2$ the entire behavior of a RW can be viewed a 1D walk along the edge with modified weight at the corner point. (This correspondence to 1D walks is explored in detail in Appendix D.)

In view of differences in the neighborhood of corner points in different lattice implementations, it is natural to assign to them a weight v that may differ from w. As in the case of a flat surface, we may inquire what choice of parameters (w, v) will create a neutral potential that admits a uniform solution $\psi_{\text{uni}}(\mathbf{r})$ to Eq. (1). In Appendix A we provide a general expression for any lattice implementation of Eq. (A9). For the geometry in Fig. 3(b) this "neutral condition" corresponds to $(w_c, v_c) = (\frac{4}{3}, 1)$. Note that the critical value of w does not change since it represents attraction along the entire wall, while the Boltzmann weight of the corner does decrease to 1, i.e., to $V^{\text{th}} = 0$, to compensate for the effective attraction caused by extra nearest neighbors. Indeed, at this particular point the N-dependent reduced partition function has a Gaussian shape as depicted in Fig. 4. This shape is very different from the RW localized to the corner at $w = v = \frac{4}{3}$, as depicted in Fig. 2(c).

For a RW anchored outside a rectangular corner, as in Fig. 3(c) the neutral point, according to Eq. (A9), is $(w_c, v_c) = (\frac{4}{3}, 2)$. As in the previous case, the critical value of w remains unchanged. However, the critical value of v increases, corresponding to increased attraction (more negative V^{th}) to compensate for effective repulsion caused by a small number of nearest neighbors.

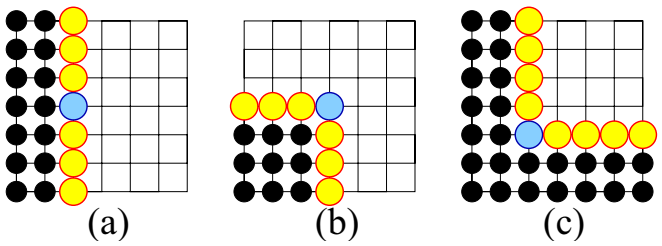

FIG. 3. The excluded sites (black circles) are bounded by an attractive layer (yellow circles) with Boltzmann weight w. The anchoring point is indicated by a blue circle, and may in principle be assigned a different weight v. The above examples include (a) straight boundary, and (b) outside and (c) inside a rectangular wedge.

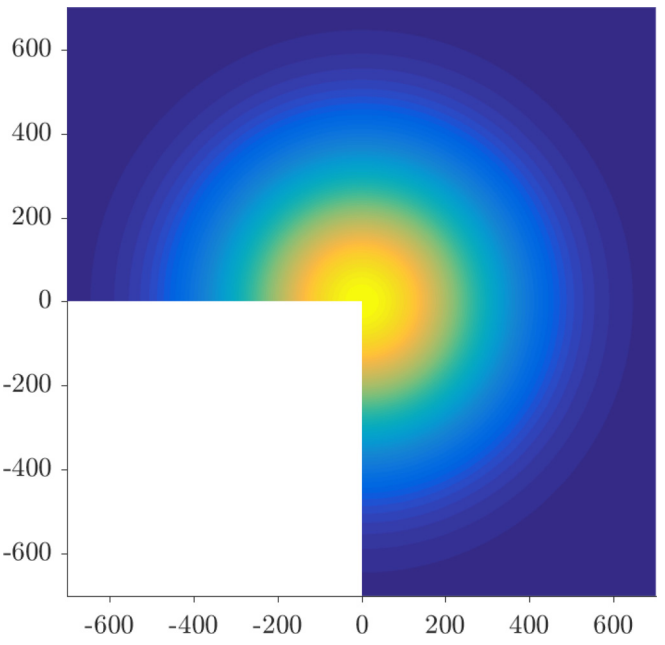

FIG. 4. Reduced partition function $\tilde{\mathcal{Z}}(\mathbf{r}, \mathbf{r}_0, N)$ for a polymer that starts at the apex $\mathbf{r}_0 = (0, 0)$ of a rectangular wedge (with full opening angle $\theta_0 = 3\pi/2$) depicted in Fig. 3(b) as a function of the polymer end position $\mathbf{r}$ for $N = 10^5$ on a discrete lattice at the neutral point $(w_c, v_c) = (\frac{4}{3}, 1)$. Outside the wedge the distribution has an undisturbed Gaussian shape.

The above problem exemplifies manifolds of different dimensionalities (edge and corner) characterized by independent Boltzmann weights w and v. In the continuum limit, this system can be mimicked by a potential $-U(\mathbf{r}) = u_1\delta(x_1) + u_2\delta(x_1)\delta(x_2)$, where (positive) u_1 and u_2 represent the potential strengths of *attraction* to the wedge and corner, respectively. Building upon Eq. (5), under RG these components (with $C = 1$ and 2, respectively) will behave as

$$\frac{d\,u_1}{d\ln b} = u_1 + \mathcal{O}(u_1^2), \tag{6}$$

$$\frac{d\,u_2}{d\ln b} = u_2^2 + \mathcal{O}(u_1 u_2). \tag{7}$$

Note that simple scaling as in Eq. (5) suggests that u_2 does not change under scaling (a marginal operator). However, as is well known in quantum mechanics, any attractive potential in two dimensions leads to a bound state. This implies that a positive u_2 is marginally relevant, captured by the added positive quadratic term [whose coefficient can be set to one by appropriate rescaling of $U(\mathbf{r})$]. While not explicitly included, we have also anticipated that the lower dimensional potential u_2 does not affect RG of the higher dimensional potential u_1, but that the reverse is allowed.

The point $u_1 = u_2 = 0$, corresponding to free diffusion, is thus unstable in two directions and corresponds to a multicritical point. In the discrete implementation, this point corresponds to $(w, v) = (\frac{4}{3}, 1)$ outside a rectangular wedge and $(w, v) = (\frac{4}{3}, 2)$ inside a rectangular wedge. We note that a similar special point can be achieved for any collection of excluded points (obstacles) for the discretized RW with the choice of $q_c(\mathbf{r})$ from Eq. (A9). In the continuum limit, this corresponds to reflecting boundary conditions at the obstacles, as noted in Ref. [18].

IV. PHASE DIAGRAMS

We undertook a detailed numerical analysis of the phase diagrams of a RW interacting with the surfaces depicted in Fig. 3, obtained on varying both the weight w of the sites adjacent to the walls and the weight v of the corner and anchor points. Technical details of the numerical approach can be found in Appendices C, D, and E. This study produced the three phase diagrams depicted in Figs. 5, 6, and 7, corresponding to the geometries in Figs. 3(b), 3(a), and 3(c), respectively. These diagrams describe the behavior of RWs at various points of the (w, v) parameter space. In all cases, for $w > w_c = \frac{4}{3}$ the RWs are localized at the walls, and for most values of w there is a critical $v_c(w)$ such that for $v > v_c$ the polymer is localized to the corner or anchor point, with no such localization for $v < v_c$. Thus, depending on the presence or absence of localization to the corner or anchor site, or to the wall, there are four possible phases. The caption of Fig. 2 explains the colors used to denote each of the four phases in all the diagrams. In the remainder of this section, we explain the details of the phase diagrams for each of the three geometries depicted in Fig. 3, casting the results in the more general perspective of phase transitions.

We first examine the phase diagram of a RW anchored to the corner of a rectangular wedge [quarter excluded space as in Fig. 2 and Fig. 3(b)] (see Appendix E for details). The presence

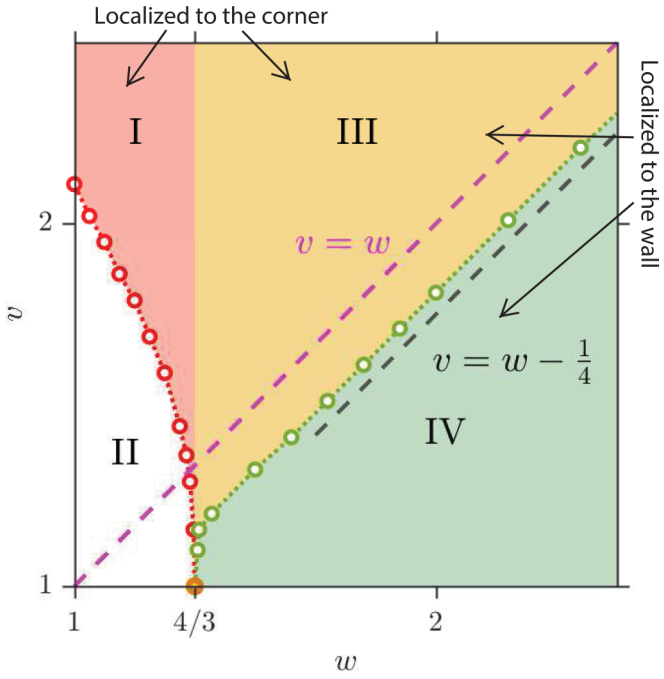

FIG. 5. Phase diagram of a RW anchored at the apex of an excluded rectangular wedge bounded by an attractive layer weighted by w, and a corner site weighted by v. There are four phases: I (pink), localized to the corner but not to the wall; II (white), delocalized from both the corner and the wall; III (light brown), localized to the corner and the wall; IV (light green), localized to the wall but not the corner. Red circles represent the numerically measured transition between phases I and II, while the green circles represent the numerically measured transition between phases III and IV; localization to the wall, which occurs for all $w > \frac{4}{3}$. The brown circle represents the multicritical point (see text). The dashed cyan line $v = w$ corresponds to the trajectory of simulations in Sec. III. The asymptotic behavior of the transition between phases III and IV at large w and v, as theoretically calculated in Appendix F, is indicated by the black dashed line.

of two relevant operators (albeit one marginally so) results in four possible phases coming together at a multicritical point as indicated in Fig. 5. The simplest characterization of the phases in this figure is whether or not there is localization to the boundary, which occurs for all $w > w_c$, corresponding to $u_1 > 0$. Integrating Eq. (6), the corresponding localization length diverges on approaching the boundary as $\xi_1 \propto u_1^{-1} \propto (w - w_c)^{-1}$.

The behavior of the localization length to the corner is more complex. When $u_1 = 0$, an attractive u_2 does lead to a bound state with a length scale ξ_2. Consistent with the marginality of u_2 in Eq. (7), this length scale diverges with an essential singularity as $\ln \xi_2 \sim u_2^{-1}$ upon vanishing attraction. A very small negative u_1 (repulsive) will grow to [following Eq. (6)] $u_1\xi_2$ over this scale. We expect localization to the corner to remain unmodified by such a repulsive wall if $|u_1|\xi_2 \ll 1$, suggesting a phase (or crossover) boundary of the form $\ln|u_1| \propto |u_2|^{-1}$. While such essential singularity is hard to pin down, the corresponding phase boundary in Fig. 5 does indeed approach $u_1 \sim (w_c - w)$ quite sharply as $u_2 \sim (v - 1) \to 0$.

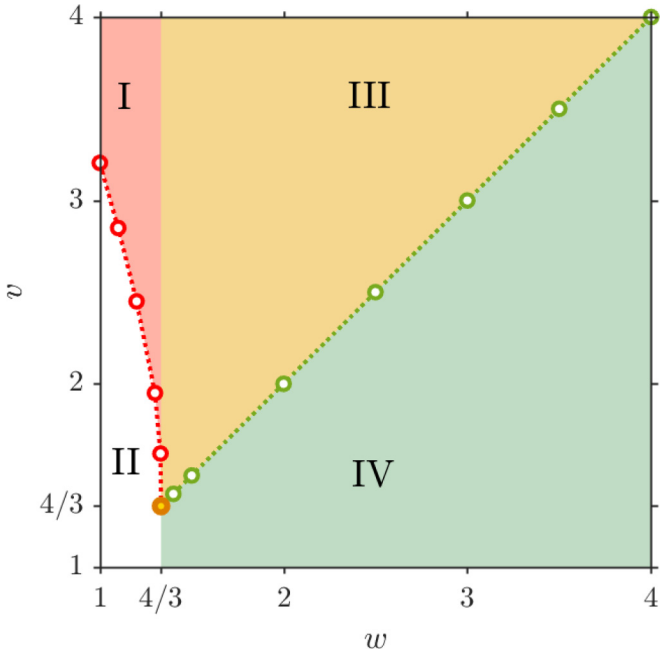

FIG. 6. Phase diagram of a RW starting from a point of weight v on a straight boundary of weight w, as depicted in Fig. 3(a). The multicritical point is at $v_c = w_c = \frac{4}{3}$, with the resulting phases and other notations as in the caption of Fig. 5.

On approaching the boundary between phases I and II, ξ_2 diverges. We expect this divergence to be asymptotically similar to that of the bound state confined by hard boundary conditions ($u_1 \to -\infty$). Such a delocalization transition was studied in Ref. [18]. Interestingly, the exponent governing the divergence of ξ_2 was found to vary continuously with the angle of the confining wedge. Within region IV of the phase diagram of Fig. 5, the RW is localized to both the edge and the corner. The RW is thus effectively constrained to move in one dimension (near the edge), experiencing an additional attraction to the corner. As this attraction weakens, the RW delocalizes from the corner, entering phase III. Taking advantage of the reduction in dimensionality, the phase boundary between regions III and IV can be computed asymptotically, as described in Appendix F. As a one-dimensional bound state, the localization length to the corner site diverges with exponent of unity on approaching this boundary.

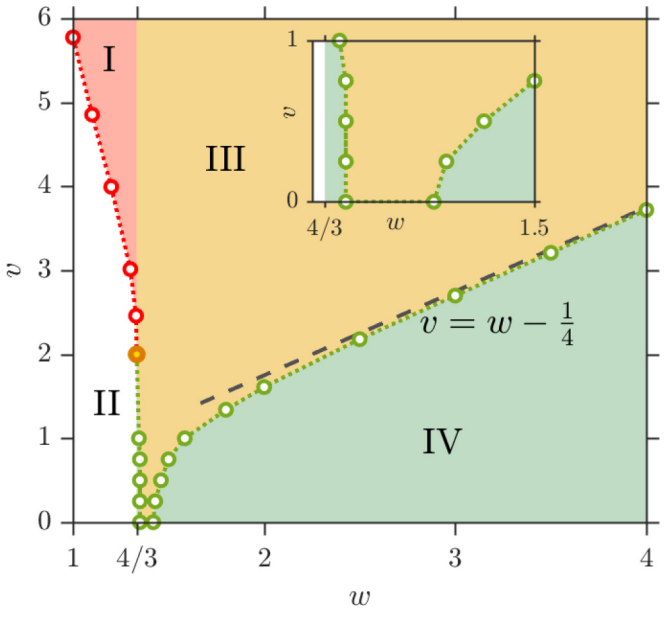

FIG. 7. Phase diagram of a RW anchored at a corner of weight v inside a rectangular wedge with boundary points of weight w, as depicted in Fig. 3(c). Phases and other notations are as in the caption of Fig. 5. The theoretically expected multicritical point is at $v_c = 2$. The numerical results indicate that a reentrant corner localized phase as w is increased for $v < v_c$, persisting to $v = 0$ (inset).

We also numerically computed phase diagrams for the other two geometries depicted in Fig. 3. The case of the favored anchored site along the straight boundary, depicted in Fig. 6, is rather simple. The anchoring site now has the same number of neighbors as any other site along the edge, and thus $v_c = w_c = \frac{4}{3}$. For any $w > w_c$, the RW is bound to the edge and is effectively one dimensional. If the anchoring point has larger weight than other points on the edge, it will localize the one-dimensional RW. Thus, the III/IV phase boundary coincides with the line $v = w$.

Finally, the phase diagram for the case of Fig. 3(c) (RW confined to the inside of a rectangular wedge) is depicted in Fig. 7. According to previous arguments, the multicritical point should occur for $v_c = 2$, as was found from Eq. (A9). Remarkably, the numerical results indicate that the corner-localized phase can persist for $v < v_c$, all the way to $v = 0$. As indicated in the inset, there is still a sliver of phase IV emerging from the multicritical point, although its boundary plunges to $v = 0$. A reentrant III/IV boundary appears for larger values of w, and asymptotes to $v = w - \frac{1}{4}$, in agreement with the arguments in Appendix G.

V. DISCUSSION

In this work we considered coexistence and competition between localized phases of (weighted) RWs to manifolds of distinct dimensions. Different weights to points on each manifold can be either assigned externally, or appear as a result of discretization leading to distinct neighborhoods. The distinct weights can lead to attraction or repulsion that may lead to localization or depletion in the vicinity of the corresponding manifold. It is, however, possible to artificially assign weights so that the manifolds become invisible to the RWs that then perform simple diffusion. For RWs on a lattice, this is achieved by the choice of weights $q(\mathbf{r}) = \mu/\mu(\mathbf{r})$, where $\mu(\mathbf{r})$ is the number of neighbors of point $\mathbf{r}$ in a lattice of coordination number μ. (In the continuum, a related condition is achieved by imposing reflecting boundary conditions at the surfaces of obstacles [18].) This choice of weights corresponds a special point in parameter space that serves as a multicritical point for manifolds of dimensions $D = d - 1$ and $d - 2$ studied in this work.

As discussed in Appendix B, ideal polymers provide a physical realization of RWs, which can be attracted or repelled by the various objects to which they are anchored. Several examples of polymers attached to scale invariant obstacles (as examples of manifolds without a characteristic macroscopic

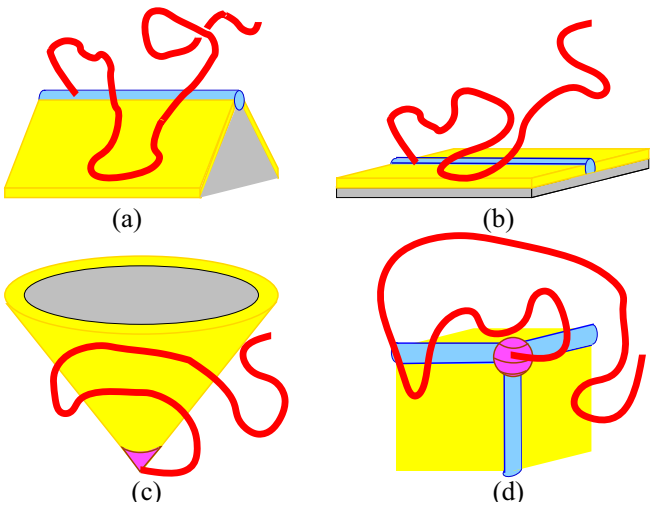

FIG. 8. Hard obstacles (gray) bounded by manifolds of dimension D two (yellow), one (blue), or zero (magenta) in $d = 3$.

scale) are depicted in Fig. 8. The wedge in Fig. 8(a) and the ridge in Fig. 8(b) are in close correspondence with the examples studied in Figs. 3(b) and 3(a), respectively. For a RW, the additional (invariant) third direction is irrelevant, while for a realistic polymer the self-avoiding interactions are expected to modify the phase diagram from those in Figs. 5 and 6 quantitatively, but not qualitatively. The apex of the cone in Fig. 8(c), or the corner of a cube in Fig. 8(d) provide realizations of manifolds of dimension $D = 0$. While these shapes are a reasonably realistic depiction of tips of atomic microscopy apparatus to which polymers can be attached, the self-avoiding condition renders the analogy to RWs problematic at these points. As a theoretical model, however, the cube in Fig. 8(d) offers the possibility of exploring a phase diagram in the presence of competing scale invariant manifolds of three distinct dimensionalities.

ACKNOWLEDGMENTS

Y.K. thanks A. Palevski and M. Goldstein for useful discussions. M.K. was supported by the National Science Foundation through Grant No. DMR-1708280, and in part by Grant No. NSF PHY 1748958 at KITP. Y.K. was supported by the Israel Science Foundation Grant No. 453/17.

APPENDIX A: WEIGHTED RANDOM WALKS ON LATTICES

Equation (1) admits an iterative solution to the problem of weighted RWs on a lattice. Regarding $\tilde{\mathcal{Z}}(\mathbf{r}', \mathbf{r}_0)$ as a column vector, this equation is equivalent to matrix multiplication

$$\tilde{\mathcal{Z}}_{N+1} = M\tilde{\mathcal{Z}}_N, \tag{A1}$$

with matrix

$$M(\mathbf{r}, \mathbf{r}') = \frac{q(\mathbf{r})}{2d}\tilde{\delta}_{\mathbf{r},\mathbf{r}'}, \tag{A2}$$

where $\tilde{\delta}_{\mathbf{r},\mathbf{r}'} = 1$ if $\mathbf{r}$ and $\mathbf{r}'$ are neighboring sites, and 0, otherwise. As mentioned in the main text, we can divide lattice sites into "even" ("e") and "odd" ("o") sublattices, depending on whether the sum of their coordinates is even or odd. Note that the matrix recursion equation indicated by Eqs. (A1) and (A2) connects "e" sites to "o" sites, while connections from "e" to "e" or "o" to "o" are absent. By applying M to Eq. (A1) we wind up with

$$\tilde{\mathcal{Z}}_{N+2} = M^2\tilde{\mathcal{Z}}_N, \tag{A3}$$

with $M^2(\mathbf{r}, \mathbf{r}') = q(\mathbf{r})\sum_{\mathbf{r}''} q(\mathbf{r}'')\tilde{\delta}_{\mathbf{r},\mathbf{r}''}\tilde{\delta}_{\mathbf{r}'',\mathbf{r}'}/4d^2$. Every nonvanishing term in this matrix sums over sites that are nearest neighbors of nearest neighbors, i.e., second neighbor sites as well as the site itself. Obviously, the matrix M^2 connects sites of the same parity, while its "o-e" elements are zero.

Note that the matrix M^2 is composed of two disconnected submatrices. We can thus find eigenstates $\psi_{\mathrm{e}}(\mathbf{r})$, with all "o" elements set to zero, that satisfy

$$\lambda^2\psi_{\mathrm{e}}(\mathbf{r}) = M^2(\mathbf{r}, \mathbf{r}')\psi_{\mathrm{e}}(\mathbf{r}'). \tag{A4}$$

Since all elements of the "e-e" submatrix are positive, it follows from the Peron-Frobenius theorem [27] that the largest modulus eigenvalue λ^2 is real positive and the eigenstate is nondegenerate. We denote this as the "ground state" and define its energy as E_0 via $\lambda^2 = \mathrm{e}^{-2E_0}$. By applying M to Eq. (A4) one more time we note that $\psi_{\mathrm{o}}(\mathbf{r}) \equiv M(\mathbf{r}, \mathbf{r}')\psi_{\mathrm{e}}(\mathbf{r}')$ is also an eigenvector with the same eigenvalue λ^2, but it has only nonvanishing "o" elements. Each eigenvalue λ^2 of Eq. (A4) corresponds to two eigenvalues $\pm\lambda$ of matrix M itself, with eigenvectors $\psi = \psi_{\mathrm{e}} \pm (1/\lambda)\psi_{\mathrm{o}}$.

In a more familiar form, the spectral structure of M in Eq. (A2) can be understood by considering a slightly modified matrix

$$M^*(\mathbf{r}, \mathbf{r}') \equiv \sqrt{q(\mathbf{r})q(\mathbf{r}')}\,\tilde{\delta}_{\mathbf{r},\mathbf{r}'}/2d, \tag{A5}$$

which is defined for $\mathbf{r}$ and $\mathbf{r}'$ on the permitted sites (with $q > 0$), acting on $\tilde{\mathcal{Z}}^*_N(\mathbf{r}) \equiv \tilde{\mathcal{Z}}_N(\mathbf{r})/\sqrt{q(\mathbf{r})}$ and reducing Eq. (A1) to

$$\tilde{\mathcal{Z}}^*_{N+1} = M^*\tilde{\mathcal{Z}}^*_N\,. \tag{A6}$$

The real symmetric matrix M^*, composed of non-negative terms, has a spectrum of real eigenvalues.

For numerical studies of polymers near attractive wells and repulsive surfaces, it is convenient to discretize to a lattice. We will consider a d-dimensional hypercubic lattice, with lattice spacing ℓ. Configurations of the polymer are now represented by N-step RWs, with a potential V^{th} assigned to every lattice site, for a Boltzmann weight $q(\mathbf{r}) = \exp(-\beta V^{\mathrm{th}})$. In free space $q = 1$, while on the repulsive wall $q = 0$. Inside, the well of depth $V^{\mathrm{th}} = -V_0^{\mathrm{th}}$, it will have weight $w = \exp(\beta V_0^{\mathrm{th}})$. The reduced $(N + 1)$-step partition function is now deduced recursively, exactly as in Eq. (1), with starting condition $\tilde{\mathcal{Z}}(\mathbf{r}, \mathbf{r}_0, 0) = q(\mathbf{r}_0)\delta_{\mathbf{r},\mathbf{r}_0}$.

Knowledge of all the eigenfunctions ψ_α, and their "energies" E_α corresponding to eigenvalues λ_α, enables reconstruction of the reduced partition function

$$\tilde{\mathcal{Z}}(\mathbf{r}, \mathbf{r}_0, N) = \sum_\alpha \psi_\alpha(\mathbf{r})\psi^*_\alpha(\mathbf{r}_0)e^{-E_\alpha N}. \tag{A7}$$

For simplicity of discussion, we shall consider even N and, consequently, the above discussion will only include the even eigenstates of M^2. If the function V^{th} represents a potential with attractive parts, we may have bound states with discrete

eigenvalues $E_\alpha < 0$, and, if there is a gap between the ground and the first excited state, for large N the solution will be dominated by the ground state $\alpha = 0$, as

$$\tilde{\mathcal{Z}}(\mathbf{r}, \mathbf{r}_0, N) \approx \psi_0(\mathbf{r})\psi_0(\mathbf{r}_0)e^{-E_0 N}. \tag{A8}$$

Since $\tilde{\mathcal{Z}}$ is positive, the ground-state function $\psi_0(\mathbf{r})$ cannot alternate in sign and can be chosen as being non-negative everywhere. When localized to an attractive potential, the eigenstate $\psi_0(\mathbf{r})$ will be highly peaked within some distance ξ near the potential. Since $\tilde{\mathcal{Z}}$ is proportional to the probability to find the RW end at $\mathbf{r}$, this means that a "polymer" will remain in close proximity of the attractive region.

On an infinite homogeneous lattice $q(\mathbf{r}) \equiv 1$ and the eigenstate of M corresponding to $\lambda_0 = 1$ or $E_0 = 0$, is the *uniform* state $\psi_{\rm uni}(\mathbf{r}) = 1$ at all sites. This can be verified by direct substitution of $\psi_{\rm uni}(\mathbf{r})$ to Eq. (A1) or (A3). In the presence of boundaries with attractive layers we can consider the same equations and the same state $\psi_{\rm uni}$, but with coordinate $\mathbf{r}$ now restricted only to allowed lattice sites [where $q(\mathbf{r}) > 0$]. The uniform solution will still be an eigenstate with $\lambda = 1$ provided $1 = \frac{q(\mathbf{r})}{2d}\sum_{\mathbf{r}' \text{ nn of } \mathbf{r}} 1 = q(\mathbf{r})\mu(\mathbf{r})/2d$, where the summation is performed only on the permitted sites $\mathbf{r}'$ neighboring any permitted site $\mathbf{r}$, and $\mu(\mathbf{r})$ is the number of such $\mathbf{r}'$s. So, selected critical values

$$q(\mathbf{r}) = q_c(\mathbf{r}) \equiv \mu/\mu(\mathbf{r}) = 2d/\mu(\mathbf{r}), \tag{A9}$$

of the attraction strengths support the uniform solution as the ground state of the system. The last part of Eq. (A9) refers to a d-dimensional hypercubic lattice; it is preceded by the result for a general regular lattice of coordination number μ. In a scale-free system, such as half-plane, we also expect the long-wavelength eigenstates to resemble those of the infinite uniform lattice. If so, the large-N solution for $\tilde{\mathcal{Z}}_N$ will be given by Eq. (2). For a planar homogeneous attractive layer of strength w on a repulsive wall, such as depicted in Fig. 1, Eq. (A9) simply reproduces Eq. (3), which for $d = 2$ gives $w_c = \frac{4}{3}$.

APPENDIX B: CORRESPONDENCE TO POLYMERS AND QUANTUM BOUND STATES

Random walks provide an idealized model of polymers, with localization to an attractive potential related to the presence of bound states for a quantum particle [28]. For a walk (polymer) with mean squared step size ℓ^2, moving in a slowly varying potential $V^{\rm th}(\mathbf{r})$, replacing spatial differences with partial derivatives, and for large N setting $\tilde{\mathcal{Z}}(\mathbf{r}, \mathbf{r}_0, N+1) - \tilde{\mathcal{Z}}(\mathbf{r}, \mathbf{r}_0, N) \approx \partial\tilde{\mathcal{Z}}/\partial N$, transforms the discrete Eq. (1) to the continuous form [22]

$$\frac{\partial\tilde{\mathcal{Z}}}{\partial N} = \frac{\ell^2}{2d}\nabla^2\tilde{\mathcal{Z}} - \beta V^{\rm th}\tilde{\mathcal{Z}}\,. \tag{B1}$$

The above equation is supplemented with the initial condition $\tilde{\mathcal{Z}}(\mathbf{r}, \mathbf{r}_0, 0) = \delta^d(\mathbf{r} - \mathbf{r}_0)$. Equation (B1) is analogous to the Schrödinger equation for a quantum particle in *imaginary time* N. The mass m, and the potential $V^{\rm q}$, of the corresponding quantum particle satisfy $d\beta V^{\rm th}/\ell^2 = mV^{\rm q}/\hbar^2$ (see Ref. [18] for additional details).

For quantitative analysis of a polymer in a potential "well," it is convenient to use dimensionless coordinates $\mathbf{r}' = \mathbf{r}/a$ where a is the typical linear dimension of the well. In terms of the Laplacian in dimensionless coordinates ∇'^2, the dimensionless potential $V \equiv \frac{2d\beta a^2}{\ell^2}V^{\rm th}$, and rescaled polymer length $N' \equiv \frac{\ell^2}{2da^2}N$, the reduced partition function satisfies

$$\frac{\partial\tilde{\mathcal{Z}}}{\partial N'} = \nabla'^2\tilde{\mathcal{Z}} - V\tilde{\mathcal{Z}} \equiv -H\tilde{\mathcal{Z}}. \tag{B2}$$

In what follows, we omit the prime in coordinate notation, and measure distances relative to the width a. The eigenvalues E'_α of H are related to those in Eq. (A7) in the same way as the potentials.

It is well known in quantum mechanics that a purely attractive potential in dimensions $d = 1$ or 2 always has at least one bound state [29,30], while in $d > 2$ the presence or absence of bound states depends on the strength and shape of the potential. In fact, if d is viewed as a continuous variable it can be shown [31] that the property of always having a bound state disappears immediately above $d = 2$, in agreement with the scaling analysis in Eq. (5). For the polymer, the relevant dimension C is the difference between the space dimension d and the dimensionality D of the attracting manifold. For example, a *three*-dimensional ideal polymer is always bound to a planar attractive layer.

The above results do not apply to potentials with both repulsive and attractive parts. For instance, a 1D potential representing an attractive layer on a repulsive wall,

$$V_{\rm wall}(x) = \begin{cases} +\infty & \text{for } x \leqslant 0, \\ -V_0 & \text{for } 0 < x < 1, \\ 0 & \text{for } x \geqslant 1, \end{cases} \tag{B3}$$

may have one or more bound states for sufficiently large V_0, but for $V_0 < U_c = \pi^2/4$ does not support any [32]. Since the dimensionless potential V_0 depends both on temperature T, as well as the strength of the actual potential $V^{\rm th}$, there is a critical value $T = T_a$ for the adsorption transition of ideal polymers to a surface covered by an attractive layer. Bound state eigenfunctions in the potential of Eq. (B3) decay exponentially as e^{-qx} outside the well, where q depends on the potential depth V_0. For an attractive potential V_0 slightly deeper than the critical value U_c, i.e., for small $\delta V_0 = V_0 - U_c$, only one bound state will be present, with $q \approx \delta V_0/2$. For sufficiently large N, the state of the polymer is governed by the ground state, its spatial extent limited by the localization length

$$\xi = 1/q = 2/\delta V_0 \sim 1/(T_a - T), \tag{B4}$$

in agreement with the scaling result of Eq. (6).

For completeness, we note that for an ideal polymer in d dimensions, adsorption to a $(d-1)$-dimensional repulsive wall covered by an attractive layer is again described by the potential $V_{\rm wall}(x_1)$ in Eq. (B3), now depending only on the coordinate x_1 perpendicular to the surface. The eigenfunctions of H behave as $\psi_{\mathbf{k}_\parallel,\alpha} = \exp[i\mathbf{k}_\parallel \cdot \mathbf{x}_\parallel]g_\alpha(x_1)$, where $g_\alpha(x_1)$ is the eigenstate of the 1D problem, and the corresponding eigenvalues (energies) are $k_\parallel^2 + E_\alpha$. While g_α represents a spectrum that is in part continuous (for $E_\alpha > 0$), and (possibly) in part discrete (for $E_\alpha < 0$, if such states are present), the spectrum of $\exp[i\mathbf{k}_\parallel \cdot \mathbf{x}_\parallel]$ is continuous. For a polymer anchored to $(0, \mathbf{x}_{\parallel 0})$, coordinates parallel to the surface spread

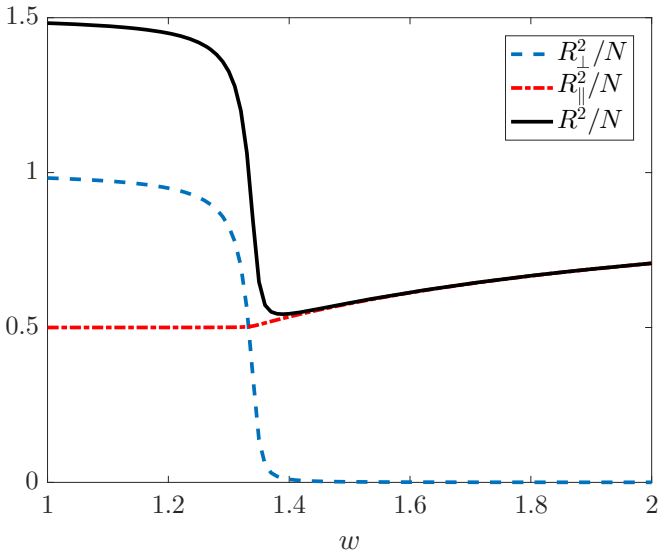

FIG. 9. Mean squared end-to-end distance perpendicular to the wall (dashed line), parallel to the wall (dotted-dashed line), and their sum (solid line), divided by polymer length of $N = 10^4$ as a function of the weight w of the attractive layer.

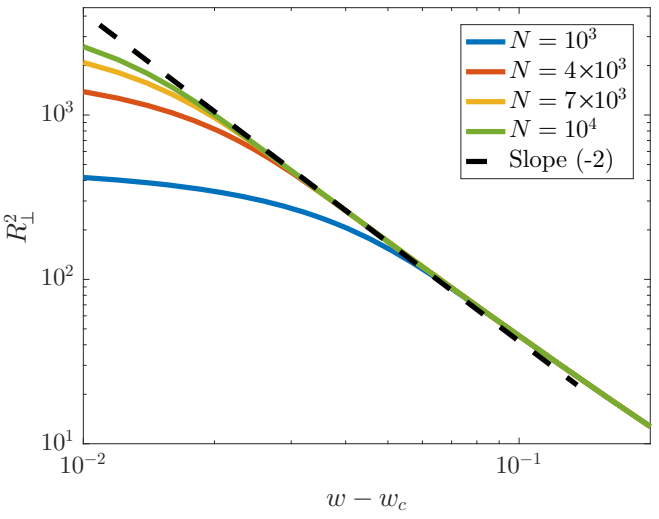

FIG. 10. Logarithmic plots of the mean squared end-to-end distance perpendicular to the wall as a function of the attractive layer weight w, for several polymer lengths N. The dashed line of slope -2 indicates the expected critical behavior near w_c for infinite N. Finite values of N cut off the critical divergence. [For bottom to top graphs (solid lines) N increases.]

diffusively, distributed $\exp[-\frac{1}{2}(\mathbf{x}_\parallel - \mathbf{x}_{\parallel 0})^2 da^2/\ell^2 N]$. The coordinate perpendicular to the surface behaves as in the 1D case discussed above, becoming localized (adsorbed) in case of a bound state.

The discrete Eq. (1) coincides with the continuum Eq. (B1) only in the limit of a weak potential with small variations between adjacent lattice sites. This is certainly not the case for a typical lattice simulation in which the geometrical features are reduced to the bare minimum, e.g., the attractive layer represented by a *single* row of weight w, as in this paper. Since the attractive layer width a now coincides with the monomer size ℓ, we can only expect qualitative similarity between the solutions of Eqs. (1) and (B1). For the discrete problem of an attractive flat layer of dimension $D = d - 1$, we obtained $w_c = 2d/(2d-1)$ in Appendix A, in agreement with the result of Rubin [20,21]. For a proper comparison between these discrete values, and $U_c = \pi^2/4$ found in the continuum, we will assume that $a = \ell$ and compare w_c with $\exp(U_c/2d)$. The former produces $w_c = 2,\ \frac{4}{3},\ \frac{6}{5}$ for $d = 1,\ 2,\ 3$, respectively, while the latter produces $3.43,\ 1.85,\ 1.51$, respectively. These are remarkably close results, considering the extreme differences between the continuous and discrete models.

APPENDIX C: ATTRACTIVE LAYER ON A FLAT SURFACE

Figure 3 depicts one flat repulsive surface, and two rectangular repulsive wedges, covered by an attractive layer of weight w. While later we allow for the corner site, to which the polymer is anchored, to have a different weight v, we first consider the one parameter case of $v = w$. The expected [20,21] localization transition at $w_c = \frac{4}{3}$ for a straight surface is easily confirmed numerically: Fig. 9 shows the w dependence of the components of the mean squared end-to-end distance. In the absence of the attractive layer for $w = 1$, the mean squared distance of the component parallel to the wall is $R_\parallel^2 = N/2$, corresponding to a 1D RW of $N/2$ steps along the wall. (This relation is exact even for small N.) For large N, the probability distribution of the component perpendicular to the wall is expected to behave as $x_1 \exp(-x_1^2/N)$. This leads to $R_\perp^2 = N$ asymptotically as $N \to \infty$; even for $N = 10^4$ this value is correct up to a few percent. In the continuum limit $R_\parallel^2$ is completely independent of w. In the lattice system, the value of $R_\parallel^2$ remains unchanged in most of the range $w < w_c$. As $w \to w_c$, $R_\perp^2$ drops from N to $N/2$, and the distribution of the end point approaches a pure Gaussian as in Eq. (2) (with $R_\perp^2 = R_\parallel^2 = N/2$). Consistent with Rubin's prediction, at w_c the configurations of the polymer resemble those of a RW near a reflecting boundary.

For $w > w_c$ the polymer is adsorbed to the surface, and $R_\perp^2$ decays rapidly with increasing w. For infinite N and close to w_c, $R_\perp^2$ is expected to diverge as $(w - w_c)^{-2}$. This is confirmed in Fig. 10, while due to finite-size effects for $0 < w - w_c < 1/\sqrt{N}$ this divergence is cut off, terminating with $R_\perp^2 = N$ at $w = w_c$. This cutoff is also clearly visible in Fig. 10.

Interestingly, for $w > w_c$ the value of $R_\parallel^2$ begins to increase contrary to the behavior of the continuous model: For large w, the walk becomes confined to the attractive layer, becoming a one-dimensional RW for $w \to \infty$ with $R_\parallel^2 = N$. This results in a nonmonotonic behavior for the total squared end-to-end distance $R^2 = R_\perp^2 + R_\parallel^2$ as observed in Fig. 9.

Figure 11 depicts the dependence of the reduced partition function $\tilde{\mathcal{Z}}_{\rm tot}$ on the polymer length N, for several values of the weight of the attractive layer. For $w = w_c$ we expect $\tilde{\mathcal{Z}}_{\rm tot} = 1$, as if the wall is completely absent. For $w > w_c$, in the adsorbed phase, $\tilde{\mathcal{Z}}_{\rm tot}$ starts increasing with N, eventually growing as an exponential, while for $w < w_c$, the value of $\tilde{\mathcal{Z}}_{\rm tot}$ decreases, eventually approaching the power-law decay ($\sim N^{-1/2}$) characteristic of a repulsive surface [33]. Note the extreme sensitivity of the large N behavior of $\tilde{\mathcal{Z}}_{\rm tot}$ to w, which

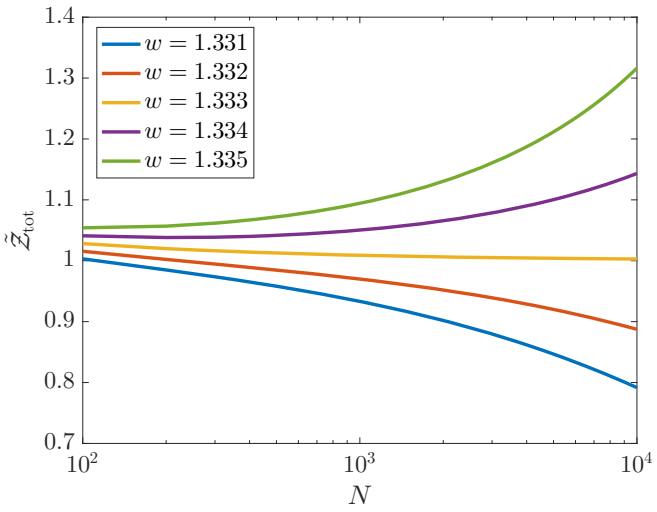

FIG. 11. Logarithmic plots of the dependence of the total reduced partition functions $\tilde{\mathcal{Z}}_{\rm tot}$ on the polymer length N for several values of w close to $w_c = \frac{4}{3}$. (For bottom to top graphs w increases.)

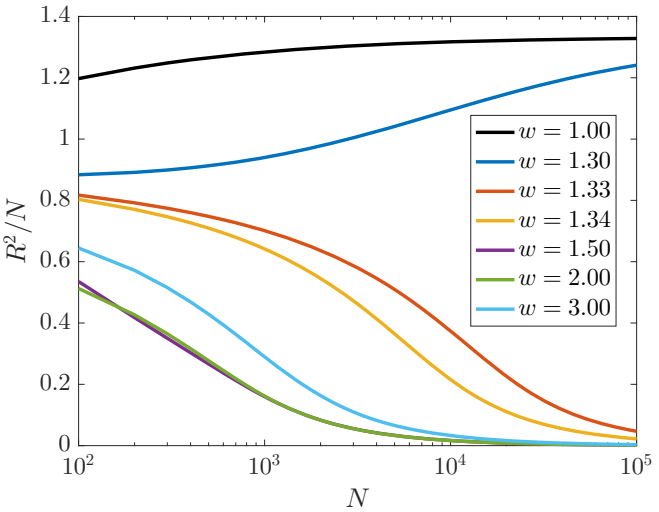

FIG. 12. Scaled mean squared end-to-end distance R^2/N, as a function of N, for several weights w. In the absence of an attractive potential ($w = 1$) the function quickly reaches the asymptotic value of $\frac{4}{3}$. For $w \geqslant 1.33$, the decay of R^2/N with increasing N signals localization. (For bottom to top of the leftmost parts of the graphs $w = 2.0$, 1.5, 3.0, 1.34, 1.33, 1.30, and 1.0, respectively.)

enables accurate numerical identification of the transition point.

Figure 1 depicts the distribution of the end point $\mathbf{r}$, proportional to $\tilde{\mathcal{Z}}(\mathbf{r}, \mathbf{r}_0, N)$, for several strengths w. Figure 1(a) corresponds to no added weight with $w = 1$. As expected for the continuum case of diffusion with adsorbing boundary conditions, this leads to a distribution $\sim x \exp[-(x^2 + y^2)/N]$, with a maximum away from the repulsive wall. As indicated before, for such a distribution, the mean squared end-to-end distance is $R^2 = \frac{3}{2}N$. With increasing w, *at fixed* N, the point of maximum approaches the wall. However, for very large N the distribution is expected to approach the same form as for $w = 1$. Indeed, even for $w = 1.3$ in Fig. 1(b), which is near the adsorption transition point, its characteristics remain practically unchanged, resembling the purely repulsive case. For $w = w_c = \frac{4}{3}$ the continuum analysis predicts a density $\sim \exp[-(x_1^2 + x_2^2)/N]$, i.e., a simple Gaussian, as in Eq. (2), truncated in the middle as seen in Fig. 1(c). Finally, in the adsorbed phase the polymer forms a narrow layer along the wall, as in Fig. 1(d) for $w = 1.8$. In this case, the parallel component is again a Gaussian distributed like a 1D RW along the boundary.

APPENDIX D: ATTRACTIVE LAYER ON A WEDGE

The wedge of full opening angle $\theta_0 = 3\pi/2$, discretized as in Fig. 3(b) with $v = w$, leads to the polymer end-point distribution depicted in Fig. 2. As shown in Refs. [34,35], for a polymer that starts at $\mathbf{r}_0$ close to the corner point of a repulsive wedge, for $N \gg r_0^2$ and for distances $r \gg r_0$,

$$\tilde{\mathcal{Z}}(\mathbf{r}, \mathbf{r}_0, N) \sim r^{2/3} e^{-r^2/N} \sin(2\theta'/3), \tag{D1}$$

where the angle θ' is measured from one of the edges. The preexponential power law increases the mean squared end-to-end size of the polymer to $R^2 = (1 + \pi/2\theta_0)N = \frac{4}{3}N$, slightly larger than that of a polymer in free space [34,35]. Figure 2(a) depicts the probability density of the end-point distribution for $N = 10^5$, which closely resembles the continuum (D1), with R^2/N within a few percent of $\frac{4}{3}$ already at $N = 10^3$ (top curve in Fig. 12). For larger w, yet below w_c we expect the same behavior for sufficiently large N. Indeed, the density distribution in Fig. 2(b), for $w = 1.3$ at $N = 10^5$, is remarkably similar to the one at $w = 1$. The ratio R^2/N again increases with N towards $\frac{4}{3}$, as seen in Fig. 12, with the second from the top curve already reaching ≈ 1.24 for $N = 10^5$.

Had the lattice realization of Fig. 3(b) with $v = w$ corresponded to reflecting boundary condition at $w = w_c$, the expected density would have been a pure Gaussian as in Eq. (2) everywhere outside the wedge. However, while the distribution in Fig. 2(c) is rotationally symmetric, it clearly shows a density centered at the origin rather than spread out over distances of order $\sqrt{N}$. A closer examination of the N dependence of R^2, as depicted in Fig. 13, shows that for $w = w_c$ and *even slightly below* w_c, R^2 approaches a *constant* for large N. Clearly, this differs from the expectations of a simple continuum theory with reflecting boundary conditions [17].

For $w > w_c$, the polymer clings to the attracting layer, the width of the adsorbed layer decreasing as for a flat surface. Already for $w = 2$, depicted in Fig. 2(d), the polymer is only a few layers away from the surface. We numerically measured the mean squared distance of the polymer end from the surface (by considering separation of the points in the fourth quadrant of Fig. 3(b) from the vertical edge), and found that already for $w = 5$, $R_\perp^2 \approx 0.2$. For larger values of w, $R_\perp^2$ decreases as $1/w$, as justified by the following argument: Assuming that $\tilde{\mathcal{Z}} = b$ for some b at the boundary, then the value of $\tilde{\mathcal{Z}}$ one lattice constant away is approximately $b/2w$. Thus, even for moderate values of w the walk is almost one dimensional. While a simple 1D N-step walk would spread over the distance $R_\parallel^2 = N$, our results indicate a much narrower distribution of the end position. This is again attributable to

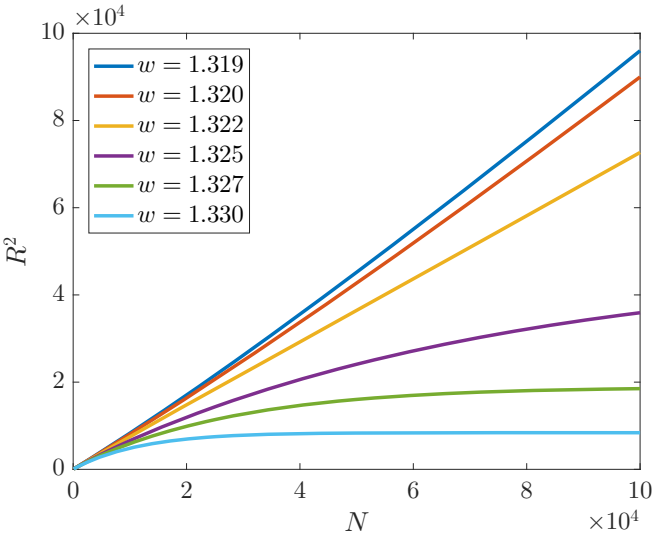

FIG. 13. R^2 as a function of N for several values of w slightly below w_c. While the topmost curve seems to represent a delocalized state, the three bottom curves approach a limiting value with increasing N. (For bottom to top graphs w decreases.)

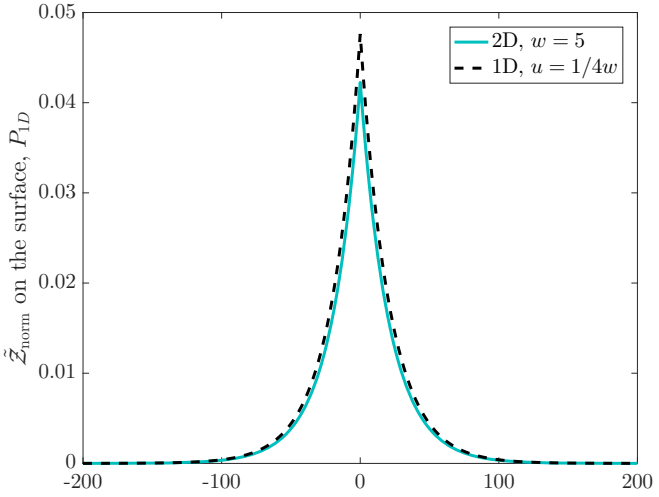

FIG. 14. The dashed line depicts the ground state P_{1D} of an ideal polymer on a 1D lattice with weight $1+u$ at the origin for $u=\frac{1}{20}$. The solid line shows the numerically calculated distribution of the 2D random walker, attracted to the wedge with $w=5$. [The graphs show only the even points corresponding to an even number of steps N ($P_{1D}=0$ at odd positions).]

an effective attraction to the corner site which has only *two* nearest neighbors away from the attractive layer [Fig. 3(b)], as opposed to a *single* neighbor for any other boundary site. Therefore, we effectively have a 1D walk with one slightly more attractive site. Since the extra attraction is coming from the sites adjacent to the attractive layer, their relative influence is $O(1/w)$, and consequently the increase of w*decreases* the contrast between the corner site and other sites along the edges.

In both the continuum and discrete cases, an attractive site always leads to a bound state in one dimension. In Appendix F we solve the 1D discrete problem with the origin given weight $1+u$ with $u>0$. The ground state behaves as $\exp(-|x|/\xi)$ with the localization length $\xi\approx 1/u$ for small u [see Eq. (F3)]. The dashed line on Fig. 14 shows the probability distribution of the end point for such a 1D polymer for $u=\frac{1}{20}$ (an exponential function with $\xi=20$). In Appendix F we find the ground state (stable distribution) of the polymer end point for a 2D problem of the wedge for $w\gg 1$, and show that it corresponds to the 1D problem with $1/u=4w$ [see Eq. (F12)]. The solid line in Fig. 14 shows the normalized probability density of the polymer end position *in the 2D problem* with $w=5$. It is also an exponential function with exactly the same width as in the corresponding 1D problem. The 2D curve is slightly lower than the corresponding 1D curve because about 5% of the probability is outside the attractive layer (most of it adjacent to that layer), and the sum of the probabilities along the layer is smaller that 1.

In Fig. 15 we compare the localization length ξ, as analytically obtained for the 1D problem above as a function of $1/u$, with the results for the 2D problem calculated from the logarithmic slope of its numerical solution (as function of $4w$). Additionally, this figure includes $\sqrt{R^2/2}$ of the 2D problem as a function of $4w$. The excellent correspondence of these results demonstrates how closely the 2D system mimics the 1D one. While the relations in Appendix F become exact for $w\gg 1$, they seem to work well even for the leftmost point in the graph corresponding to $w=2$.

It is interesting to note a nonmonotonic behavior in Fig. 12: As w increases from 1.33 to 1.5 the graphs plunge down more rapidly, indicating shorter localization lengths. This trend is halted at $w=2$, and reversed for $w=3$, indicating a longer localization length which continues to grow for even larger values of w in Fig. 15. This is a manifestation of the crossover to almost 1D behavior for $w\gtrsim 2$ which leads to weaker 1D localization to the corner with *increasing* w, from

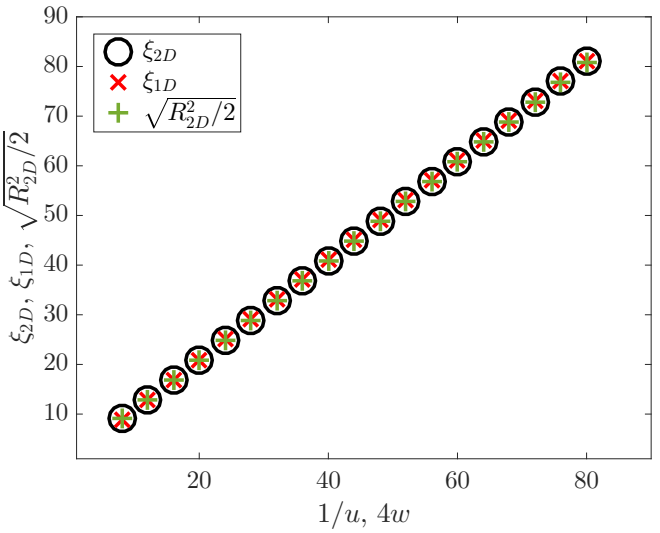

FIG. 15. Comparison of numerically measured correlation lengths of a 1D walk with attractive point of weight $1+u$, as a function of $1/u$, and that of a 2D walk localized to a wedge, as a function of $4w$.

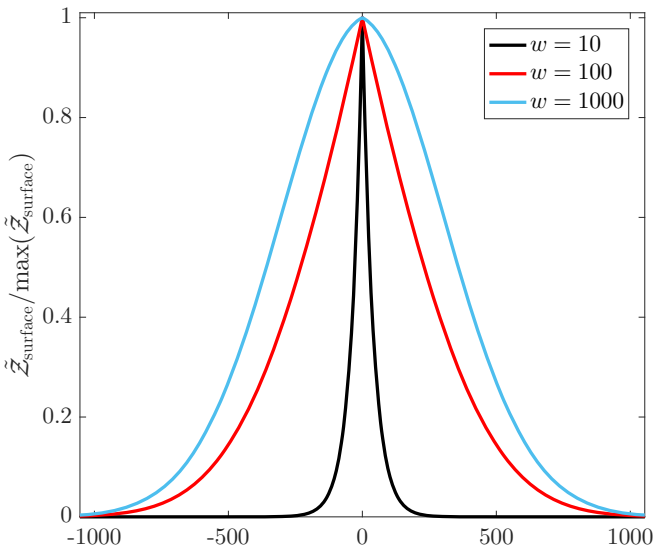

FIG. 16. Numerically measured normalized $\tilde{\mathcal{Z}}$ as a function of distance from the corner, obtained for several values of w with the weight of the corner site set to 1. ($\tilde{\mathcal{Z}}_{\rm norm}$ is included only at even positions, vanishing for odd sites.) For $w = 10$, the function decays exponentially with distance from the corner. For $w = 100$ it deviates from a simple exponential, while for $w = 1000$ it closely resembles a Gaussian, except for a slope discontinuity at the origin.

"2D-like" behavior for $w \lesssim 1.5$ where localization weakens with *decreasing* w.

Numerical results for the ground state presented in this section were obtained by iterating Eq. (1), rather than solving Eq. (A4), relying on the fact that in the presence of a bound state the distribution approaches the ground state at *sufficiently large* N. For $N = 10^5$, a polymer in free space expands over a distance of $\sqrt{N} \approx 320$. When the localization length of the ground state is $\xi \ll 320$, there is no issue with finite N. However, as $\xi \approx 4w$, for $w \gtrsim 80$, $N = 10^5$ no longer ensures approach to the ground state. The probability density thus obtained in the boundary layer, depicted in Fig. 16, does indeed show an exponential decay with $\xi = 40$ for $w = 10$, but strongly deviates from such for $w = 100$, due to finite-size effects. Finally, for $w = 1000$, the walker is very weakly bound in its ground state, with an expected localization length of $\xi = 4000$. In this case the finite-N distribution does not resemble the ground state, and looks almost as a Gaussian in free space, with a slight deviation near the origin, where a discontinuity in the derivative portends the expectation of a bound state.

APPENDIX E: PHASE DIAGRAM NEAR A WEDGE

As apparent in Fig. 2(c), the polymer is localized to the corner for $v = w = w_c$ with $\sqrt{R^2} \approx 90$. Moreover, even slightly below w_c, there is a finite localization length, possibly up to $w \approx 1.32$. As discussed in the text, the "neutral" condition is only obtained by assigning the corner a weight $v \neq w$. In an earlier work [18] we explored the behavior of a polymer anchored to the attractive corner site ($v > 1$) of a repulsive wedge ($w = 1$), finding a transition to a corner-localized state for $v = v_c = 2.109$. In this Appendix, we discuss the more general phase diagram in the (w, v) plane, as depicted in Fig. 5.

The model allows for four different phases depending on whether the polymer is adsorbed (desorbed) to (from) the corner, and adsorbed (desorbed) to (from) the edge. The simulations presented in Appendix D were performed along the line $v = w$ indicated by the dashed cyan line in Fig. 5.

For $w < w_c$ the surface attraction is too weak to localize the polymer. However, as w increases from 1 to $\frac{4}{3}$ the critical value v_c of adsorption to the corner decreases since weaker repulsion from the edge facilitates localization to the corner. The dotted red line in Fig. 5 represents this localization transition to the corner. Simulations along $v = w$ in Appendix D indicated the presence of a localized state until $w \approx 1.32$. Thus, the red line passes slightly to the left of $w = w_c$. By examining the N dependence of R^2 and $\tilde{\mathcal{Z}}_{\rm tot}$ we located several transition points between the localized and delocalized state for $w < w_c$ and the results determined this boundary in Fig. 5.

The numerical results in Figs. 11 or 12 or 13 are almost exact since they are determined by an exact iteration of Eq. (1), and only minute and well controlled errors are introduced by the finite-size corrections. The transition points in these figures are obtained from the asymptotic behavior of various curves beyond the "small-N" crossovers, which may continue even to $N = 10^5$ and beyond, leading to systematic errors. Typically, the transition point was located by keeping one of the parameters fixed (w or v, for small- or large-slope segments of the transition line, respectively) and changing the other parameter in small increments. The N dependence of polymer size or the reduced partition function was measured at each such point (w, v). Our subjective estimate is that the systematic errors are of the order of the size of symbols denoting the transition points.

As discussed in the main text and in Appendix A, a neutral point is obtained by assigning weights $q(\mathbf{r})$ such that $\psi_{\rm uni}$ is an eigenstate of eigenvalue $\lambda = 1$. In accordance with Eq. (A9) for the excluded (quarter) wedge, this corresponds to $(w, v) = (\frac{4}{3}, 1)$. Indeed, iteration of Eq. (1) for these values leads to a Gaussian distribution of the polymer end point as depicted in Fig. 4. We expect this to be the terminal point of the red line in Fig. 5, and note the almost vertical entrance of this line to the neutral point.

For $w > w_c$ the polymer is adsorbed to the attractive wedge, but may or may not be localized to its corner. As discussed in Appendix F [see Eq. (F13)] for large w, the polymer will delocalize from the corner at $v \approx w - \frac{1}{4}$. This asymptote is depicted by a black dashed line in Fig. 5. The green dotted line depicts this transition as found by examining the numerically calculated N dependence of R^2, as well as by examining entire distributions of end points for large N. Such distributions are expected to be peaked at the corner in corner-localized states, and depleted near the corner, while still clinging to the surface, in surface-localized states. We found that for moderate values of w ($\sim$2) the transition appears slightly ($\sim$0.05) above the $v = w - \frac{1}{4}$ asymptote. For small w we expect the transition line to terminate at the multicritical point $(w_c, v_c) = (\frac{4}{3}, 1)$.

Similar analysis was performed for the other geometries in Fig. 3. For the straight edge in Fig. 3(a), since the anchoring point does not differ from the rest of the surface, the neutral

point is located at $(w_c, v_c) = (\frac{4}{3}, \frac{4}{3})$. At this point, the N-dependent solution is a pure Gaussian, as in Fig. 1(c). For $w < w_c$ the line separating states bound or unbound to the corner is depicted by the dotted red line in Fig. 6. It passes through the point $(w, v) = (1, 3.205)$ found in [18], decreases with increasing w, and terminates at the multicritical point $(w_c, v_c) = (\frac{4}{3}, \frac{4}{3})$. For $w > w_c$, the distribution becomes increasingly 1D with increasing w. As long as $v = w$, its neighborhood is no different from other locations along the surface. For $v > w$ (or $v < w$) the anchoring becomes more attractive (or repulsive) leading to localization (or expulsion). Adsorption to the anchor point for $w > \frac{4}{3}$ at $v = w$ is confirmed numerically at the dotted green line in Fig. 6.

The phase diagram of a polymer confined to the inside of the rectangular wedge, as in Fig. 3(c), proved much more difficult to obtain numerically. When the attractive layer is absent, the anchor point is well shielded by the repulsive surface, and a strong attraction of $v = v_c = 5.776$ [18] is needed for localization. With increasing w, the red points for v_c decrease, ending at the neural point $(w_c, v_c) = (\frac{4}{3}, 2)$ as depicted in Fig. 7. For large w, the polymer again becomes effectively 1D, and the corresponding 1D localization is discussed in Appendix G. The boundary between corner-localized and delocalized states is found to approach $v = w - \frac{1}{4}$ [see Eq. (G7)] for large w, rather surprisingly coinciding with the asymptotic form [Eq. (F13)] for a polymer anchored to the corner *outside* a rectangular wedge. Numerical results (green dotted line in Fig. 7) indeed confirm this behavior. The more surprising numerical result is the reentrant behavior observed upon increasing w. At $w \approx 1.45$ the line reaches $v = 0$, i.e., when the corner site is infinitely repulsive.

APPENDIX F: QUASI-1D BEHAVIOR OUTSIDE A WEDGE

Consider an ideal polymer on a regular 1D lattice, with the weights $q(x) = 1$ of all sites $x \neq 0$, and $q(0) = 1 + u$. With attraction to the origin for $u > 0$, the 1D problem always supports a bound state $\psi(x)$, which following Eq. (A4), satisfies

$$\lambda\psi(x) = \frac{q(x)}{2}[\psi(x+1) + \psi(x-1)]. \tag{F1}$$

Depending on x, Eq. (F1) takes two forms

$$\lambda\psi(x) = \frac{1}{2}[\psi(x+1) + \psi(x-1)], \text{ for } |x| \geqslant 1 \tag{F2a}$$

$$\lambda\psi(0) = \frac{1+u}{2}[\psi(1) + \psi(-1)]. \tag{F2b}$$

It is easily verified that the ground state is $\psi(x) = e^{-|x|/\xi}$, where ξ is the localization length of the bound state. Substituting this into Eqs. (F2) leads to $\lambda = (1+u)e^{-1/\xi}$, and $\xi = 2/\ln(1+2u)$. When the attraction is weak, for $u \ll 1$, the correlation length becomes

$$\xi \approx 1/u. \tag{F3}$$

We are not aware of a solution to Eq. (A4) for the full 2D problem in Fig. 3(b). However, when the Boltzmann factor w is *very large*, the polymer density is concentrated on the attractive layer, and a perturbative solution is possible, as the values of the eigenfunction on the adjacent layer are smaller by $O(1/w)$, and $O(1/w^2)$ on the subsequent layer. As such, we focus on the first two layers, describing the eigenstate by it values $\psi_a(x)$ on the attracting layer, and $\psi_b(x)$ in the adjacent layer, neglecting further layers where values of the eigenvector are of order $1/w^2$. In this 1D problem, every layer "a" site with $|x| \geqslant 1$ has *one* neighbor in layer "b," while the corner site ($x = 0$) has *two* neighbors in layer "b," and therefore is effectively slightly more attractive than other sites. Furthermore, the Boltzmann weight of the corner site v differs from w. [Self-consistently in the large w limit, relevant v do not differ from w by more than a constant, and therefore in the calculation the approximation $O(1/w^2)$, also implies $O(1/v^2)$.] It is convenient to rescale the eigenvalue as $\frac{w}{2}\lambda \equiv e^{-E}$, where $\frac{w}{2}$ represents the trivial shift on an attractive layer. For $|x| \geqslant 1$ applying Eq. (A4) to two layers results in

$$\frac{w}{2}\lambda\psi_a(x) = \frac{w}{4}[\psi_a(x+1) + \psi_a(x-1) + \psi_b(x)], \tag{F4a}$$

$$\frac{w}{2}\lambda\psi_b(x) = \frac{1}{4}[\psi_b(x+1) + \psi_b(x-1) + \psi_a(x)]. \tag{F4b}$$

Equation (F4b) disregards the presence of the third layer, and therefore is missing terms of order $\psi_a(x)/w^2$. It connects ψs in two layers by $\psi_b(x) = \frac{1}{2w\lambda}\psi_a(x) + O(1/w^2)$. Substituting this result into Eq. (F4a) we arrive at

$$\psi_a(x)\left(\lambda - \frac{1}{4w\lambda}\right) = \frac{1}{2}[\psi_a(x+1) + \psi_a(x-1) + O(1/w^2)], \tag{F5}$$

which closely resembles Eq. (F2a). If we assume that the ground state is purely exponential, i.e., $\psi_a(x) = e^{-|x|/\xi}$, then Eq. (F5) immediately connects λ and the localization length as

$$\lambda - \frac{1}{4w\lambda} = \cosh(1/\xi) + O(1/w^2). \tag{F6}$$

When both w and ξ are large, this relation simplifies to

$$\lambda = 1 + \frac{1}{4w} + O\left(\frac{1}{w^2}, \frac{1}{\xi^2}\right). \tag{F7}$$

The corner sites lead to a different set of equations

$$\frac{w}{2}\lambda\psi_a(0) = \frac{v}{4}[2\psi_a(1) + 2\psi_b(0)], \tag{F8a}$$

$$\frac{w}{2}\lambda\psi_b(0) = \frac{1}{4}\{\psi_b(1) + \psi_a(0)[1 + O(1/w^2)]\}, \tag{F8b}$$

where we noted that the solution is symmetric around the origin. From Eq. (F8b) we find $\psi_b(0) = \frac{1}{2w\lambda}\psi_a(0) + O(1/w^2)$, which when substituted into Eq. (F8) yields

$$\psi_a(0)\left[\lambda - \frac{v}{2w^2\lambda} + O\left(\frac{1}{w^2}\right)\right] = \frac{v}{w}\psi_a(1). \tag{F9}$$

Assuming the exponential solution leads to

$$\lambda - \frac{v}{2w^2\lambda} = \frac{v}{w}e^{-1/\xi} + O(1/w^2). \tag{F10}$$

From Eq. (F7) with Eq. (F10) we find (at leading order)

$$\xi \simeq 4w. \tag{F11}$$

By comparing the values of ξ for the 1D problem in Eq. (F3) with the similar solution in the 2D problem, we establish the

correspondence

$$\frac{1}{u} \simeq 4w, \tag{F12}$$

relating the strong w regime of the 2D problem to the weak attraction limit of the 1D problem.

A finite ξ confirms the expectation that a slightly more attractive corner leads to localization. However, by decreasing the weight v of the corner we can effectively turn it into a repulsive potential. By examining the relations between v, w, λ, and ξ in the limit of *large* w and v, we may inquire as to how much v should be decreased to produce $\xi = \infty$? We find that this occurs for

$$v = w - \frac{1}{4} + O\left(\frac{1}{w}\right), \tag{F13}$$

with λ as in Eq. (F7). Thus, for large w a slight decrease in v will delocalize the state from the corner.

APPENDIX G: QUASI-1D BEHAVIOR INSIDE A WEDGE

In this Appendix we employ the same procedure as in Appendix F to study the polymer *inside* a rectangular wedge as in Fig. 3(c) for very large w. We again use a single coordinate x measured along the boundary from the corner, and use indices (a, b) to denote the boundary layer or the one adjacent to it. We will assume that the eigenstate ψ in negligible beyond these first two layers, and use the same approximations as in Appendix F.

For $|x| \geqslant 2$ the eigenvalue equations are identical to Eq. (F4), and for exponentially decaying solutions the same relations as in Eqs. (F6) and (F7) hold. The corner site ($x = 0$) neighbors two sites on the attractive boundary and has no neighbors on the adjacent layers. Therefore, the equation for this site is

$$\frac{w}{2}\lambda\psi_a(0) = \frac{v}{4}[\psi_a(1) + \psi_a(-1)], \tag{G1}$$

which assuming a symmetric solution immediately yields

$$\psi_a(0) = \frac{v}{\lambda w}\psi_a(1). \tag{G2}$$

The set of equations (F4) for $|x| = 1$ is now also special: While Eq. (F4a) remains unchanged, Eq. (F4b) is modified because the site at $x = 1$ at layer "b" has *two* neighbors belonging to layer "a," resulting in

$$\frac{w}{2}\lambda\psi_a(1) = \frac{w}{4}[\psi_a(0) + \psi_a(2) + \psi_b(1)], \tag{G3a}$$

$$\frac{w}{2}\lambda\psi_b(1) = \frac{1}{4}[2\psi_b(2) + 2\psi_a(1)]. \tag{G3b}$$

Equation (G3b) connects ψs in two layers: $\psi_b(1) = \frac{1}{w\lambda}\psi_a(1) + O(1/w^2)$. By substituting this result into Eq. (G3a) and using Eq. (G2), we arrive at

$$\psi_a(1)\left(\lambda - \frac{1+v}{2w\lambda}\right) = \frac{1}{2}[\psi_a(2) + O(1/w^2)], \tag{G4}$$

which, for an exponential solution, relates λ and ξ as

$$\lambda - \frac{1+v}{2w\lambda} = \frac{1}{2}e^{-1/\xi} + O(1/w^2). \tag{G5}$$

We begin examination of Eqs. (G5) and (F6) for the case of $v = w \gg 1$. We use Eq. (F7) with Eq. (G5) to find to the first order that

$$\xi = 4w. \tag{G6}$$

Once more, decreasing the weight v of the corner can effectively make it repulsive. Examination of the relations between v, w, λ, and ξ in the limit of *large* w and v regime, indicates that this occurs at

$$v = w - \frac{1}{4} + O\left(\frac{1}{w}\right). \tag{G7}$$

Thus, for large w a decrease in v by the same amount as in Eq. (F13) of Appendix F will delocalize the state from the corner, spreading it along the attractive edge.

[1] B. D. Hughes, *Random Walks and Random Environments*, Vol. 1 (Clarendon, Oxford, 1995).

[2] J. Rudnick and G. Gaspari, *Elements of Random Walk* (Cambridge University Press, Cambridge, 2004).

[3] P.-G. de Gennes, *Scaling Concepts in Polymer Physics* (Cornell University Press, Ithaca, New York, 1979).

[4] E. Eisenriegler, K. Kremer, and K. Binder, J. Chem. Phys. **77**, 6296 (1982).

[5] K. Binder, in *Phase Transitions and Critical Phenomena*, Vol. 8, edited by C. Domb and J. L. Lebowitz (Academic, London, 1983), pp. 1–144.

[6] K. De'Bell and T. Lookman, Rev. Mod. Phys. **65**, 87 (1993).

[7] S. Livne and H. Meirovitch, J. Chem. Phys. **88**, 4498 (1988).

[8] H. Meirovitch and S. Livne, J. Chem. Phys. **88**, 4507 (1988).

[9] H. Meirovitch and I. Chang, Phys. Rev. E **48**, 1960 (1993).

[10] E. Eisenriegler, *Polymers near Surfaces* (World Scientific, Singapore, 1993).

[11] T. Vrbová and S. G. Whittington, J. Phys. A: Math. Gen. **31**, 3989 (1998).

[12] G. Rychlewski and S. G. Whittington, J. Stat. Phys. **145**, 661 (2011).

[13] P. G. de Gennes, Macromolecules **14**, 1637 (1981).

[14] E. J. Janse van Rensburg, *The Statistical Mechanics of Interacting Walks, Polygons, Animals and Vesicles*, 2nd ed. (Oxford University Press, Oxford, 2015).

[15] M. F. Maghrebi, Y. Kantor, and M. Kardar, Europhys. Lett. **96**, 66002 (2011).

[16] M. F. Maghrebi, Y. Kantor, and M. Kardar, Phys. Rev. E **86**, 061801 (2012).

[17] Y. Kantor and M. Kardar, Phys. Rev. E **96**, 022148 (2017).

[18] R. Halifa Levi, Y. Kantor, and M. Kardar, Phys. Rev. E **96**, 062132 (2017).

[19] T. E. Fisher, P. E. Marszalek, A. F. Oberhauser, M. Carrion-Vazquez, and J. M. Fernandez, J. Physiol. **520**, 5 (1999).

[20] R. J. Rubin, J. Chem. Phys. **43**, 2392 (1965).
[21] R. J. Rubin, AIP Conf. Proc. **109**, 73 (1984).
[22] F. W. Wiegel, *Introduction to Path-Integral Methods in Physics and Polymer Science* (World Scientific, Singapore, 1986).
[23] J. Cardy, *Scaling and Renormalization in Statistical Physics* (Cambridge University Press, Cambridge, UK, 1996).
[24] J. Zinn-Justin, *Phase Transitions and Renormalization Group* (Oxford University Press, Oxford, UK, 2007).
[25] W. D. McComb, *Renormalization Methods* (Oxford University Press, Oxford, UK, 2004).
[26] M. Kardar, *Statistical Physics of Fields* (Cambridge University Press, Cambridge, 2007).
[27] C. D. Meyer, *Matrix Analysis and Applied Linear Algebra* (SIAM, Philadelphia, 2000).
[28] P.-G. de Gennes, Rep. Prog. Phys. **32**, 187 (1969).
[29] L. D. Landau and E. M. Lifshitz, *Quantum Mechanics (Non-Relativistic Theory)*, 3rd ed., Course of Theoretical Physics No. 3 (Elsevier, Amsterdam, 2005).
[30] K. Chadan, N. N. Khuri, A. Martin, and T. T. Wu, J. Math. Phys. **44**, 406 (2003).
[31] M. M. Nieto, Phys. Lett. A **293**, 10 (2002).
[32] L. I. Schiff, *Quantum Mechanics* (McGraw-Hill, New York, 1955).
[33] S. Chandrasekhar, Rev. Mod. Phys. **15**, 1 (1943).
[34] Y. Hammer and Y. Kantor, Phys. Rev. E **89**, 022601 (2014).
[35] N. Alfasi and Y. Kantor, Phys. Rev. E **91**, 042126 (2015).